Effective GAI is best estimated from reflectance observations as compared to GAI and LAI: Demonstration for wheat and maize crops based on 3D radiative transfer simulations

Jingyi Jiang, Marie Weiss, Shouyang Liu, Frédéric Baret

Effective GAI is best estimated from reflectance observations as compared to GAI and LAI: demonstration for wheat and maize crops based on 3D radiative transfer simulations

Jingyi Jiang[a,b], Marie Weiss[b], Shouyang Liu[c,b], Frédéric Baret[b]

[a] The Key Laboratory for Silviculture and Conservation of Ministry of Education, Beijing Forestry University, Beijing Forestry University, 100083 Beijing, China

[b] INRAE, Avignon Université, UMR EMMAH, F-84000, Avignon, France

[c] PheniX, Academy for Advanced Interdisciplinary Studies, Nanjing Agricultural University, Nanjing 210095, China

Abstract

The definition of LAI (Leaf Area Index) is important when deriving it from reflectance observation for model application and validation. Canopy reflectance and the corresponding quantities of LAI, PAI (Plant Area Index), GAI (Green Area Index) and effective GAI (GAI_{eff}) are first calculated using a 3D radiative transfer model (RTM) applied to 3D wheat and maize architecture models. A range of phenological stages, leaf optical properties, soil reflectance, canopy structure and sun directions is considered. Several retrieval methods are compared, including vegetation indices (VIs) combined with a semi-empirical model, and 1D or 3D RTM combined with a machine learning inversion approach. Results show that GAI_{eff} is best estimated from remote sensing observations. The RTM inversion using a 3D model provides more accurate GAI_{eff} estimates compared with VIs and the 1D PROSAIL model with RMSE = 0.33 for wheat and RMSE= 0.43 for maize. GAI_{eff} offers the advantage to be easily accessible from ground measurements at the decametric resolution. It was therefore concluded that the most efficient retrieval approach would be

to use machine learning algorithms trained over paired GAI_{eff} and the corresponding canopy reflectance derived either from realistic 3D canopy models or from experimental measurements.

Highlights

- Wheat and maize canopy reflectance are simulated with realistic 3D model
- Effective GAI is best estimated from remote sensing observations
- 3D model provides the best estimation of effective GAI compared to 1D model and VIs

Key words

effective GAI, wheat, maize, 3D radiative transfer model, canopy reflectance

1 Introduction

Leaf area index (LAI) was defined by Chen and Black (1992) as half the total developed area of leaves per unit horizontal ground area. LAI is directly involved in vegetation functioning and is therefore widely used in agriculture, ecology or global change research and application domains. As leaves represent the main boundary between the plant and the atmosphere, LAI is a key variable used to evaluate the exchanges of mass and energy (Liang 2004). Furthermore, it reflects the actual plant state and its potential growth (Gonsamo 2009). However, depending on the targeted traits and processes, several definitions of LAI are used:

- For the aboveground biomass estimation based on allometric relationships (Baret et al. 1989), LAI from the Chen and Black’s definition (1992) is relevant. Note that the Green Leaf Area Index (GLAI) is often used in place of LAI, by considering only the green parts of the leaves.
- For the rainfall interception efficiency of the canopy, all the vegetation elements including leaves, stems, branches and the other aerial organs, either green or senescent should be considered (Domingo et al. 1998; Martello et al. 2015). This leads to using the Plant Area Index (PAI).

- For transpiration and photosynthesis, all the green parts that potentially exchange carbon and water mainly through the stomata should be considered (Wang and Dickinson 2012). The Green Area Index (GAI) should be used in this case.
- When estimating the radiation interception efficiency, the spatial arrangement of green vegetation elements needs to be considered since leaf clumping may reduce the interception efficiency by the mutual masking of elements, leading to the effective GAI (GAI_{eff}) definition. GAI_{eff} may be defined as the GAI value of a turbid medium canopy that would provide the closest green fraction to that of the canopy considered.

These different quantities are closely related, while their relationship will depend on the species, canopy state, and stage. It is therefore mandatory to use the appropriate quantity to ensure a high degree of consistency the targeted application.

Under field conditions, LAI (and GLAI) can be only accessed using direct methods where the (green for GLAI) area of individual leaves is measured for all the leaves present over a given ground area. Similarly, PAI can be measured directly by including the area of all the other elements while only the green parts will be considered for GAI. However, these direct methods are tedious, low-throughput, and generally destructive or at least invasive. This explains why indirect methods are widely used (Gower et al. 1999). Indirect methods are based on instruments measuring canopy gap fraction (the fraction of background sun seen in a given direction) or green fraction (the fraction of green area covered in a given direction) using the same theory that relates the area of canopy elements to the gap (or green) fraction (Jonckheere et al. 2004). The simplest techniques are based on canopy transmittance measurements placed at the bottom of the canopy and used as a proxy of the gap fraction. Hemispherical light sensor (Leblanc et al. 2005), mono-directional sensor (Brede et al. 2018), or multidirectional sensors such as LAI2000 instrument (Campbell and Norman 1988) or upward looking digital hemispherical photography (Demarez et al. 2008) are widely used. Those techniques where the sensor is put at the bottom of the canopy, are sensitive to the presence of both green and non-green elements without the possibility to separate them. They provide thus a proxy of PAI (Norman and Campbell 1989). Conversely, techniques based on cameras looking downward from above the canopy allows identifying the green pixels from which GAI is derived. Mono-directional (Baret et al. 2010) or multi-directional (Weiss et al. 2004) views can be used. More recently terrestrial laser scanners (Liu et al. 2017; Soma et al. 2018; Yan et al. 2019) or stereovision (Biskup et al. 2007) have been also used to build a 3D point cloud from which the directional canopy transmittance is computed. This leads to estimates of PAI if no distinction is made between the green and non-green elements, or to GAI when the green points are identified.

The transformation of the measured directional gap or green fraction into PAI or GAI is generally based on some assumptions on canopy structure, particularly regarding leaf arrangement. One of the main assumptions considers that leaves are randomly distributed within the canopy volume. A distinction is thus made between the true PAI or GAI and the corresponding “effective” values that are derived from gap or green fraction measurements assuming that leaves are randomly distributed (Fang et al. 2018; Nilson 1999).

PAI and GAI can also be retrieved from reflectance observations using empirically or physically based methods. Empirical methods consist in calibrating relationships between a combination of reflectance in several wavebands and ground measured LAI. The most common method is the use of spectral vegetation indices (VIs) (Broge and Leblanc 2001; Broge and Mortensen 2002; Liu et al. 2012; Richardson et al. 1992). While in the past, empirical methods were calibrated, and thus, applicable over very restricted experiments and environmental conditions, recent developments have shown that robust and accurate estimates can be assessed with machine learning techniques providing that the data used to train the algorithms represents well the domain of application (Camacho et al. 2017). Conversely, physically based methods consist in inverting a Radiative Transfer Model (RTM) that simulates the physical processes involved in the photon transport within the canopy (Strahler 1997). Inversion techniques such as optimization (Jacquemoud et al. 2000), Look-Up-Tables (LUT) (Duan et al. 2014; González-Sanpedro et al. 2008) or machine learning (Verrelst et al. 2012; Weiss et al. 2002) are used to estimate the RTM input variables including PAI or GAI from the measured reflectances. The accuracy of such methods depends on the ability of the model to simulate realistically the reflectance of the targeted canopy given a description of the architecture of the canopy and the optical properties of its elements. The 1D RTMs such as PROSAIL (Jacquemoud et al. 2009) assume that the canopy is a horizontally homogeneous layer of randomly distributed leaves. Inverting 1D RTMs has the advantage of being computationally efficient and characterized by a low number of inputs, which eases the setting of numerical experiments and constrains the possible ambiguities between variables during the inversion process (Baret and Buis 2008). However, several 3D radiative transfer models were developed to get more realistic simulations of canopy reflectance: they combine an explicit 3D description of the canopy architecture while accounting for the differences in optical properties of the several vegetation elements. 3D RTMs such as FLIGHT (North 1996) based on Monte Carlo ray tracing methods or DART (Gastellu-Etchegorry et al. 2004) based on the discrete ordinate methods have already been used to retrieve canopy structure and biochemical variables from remote sensing data (Banskota et al. 2015; Gascon et al. 2004; Hernández-Clemente et al. 2017; Malenovský et al. 2013). Such 3D models are inverted using LUT or machine learning techniques. However, compared to 1D RTMs, the large computation effort required to populate the LUT or the training dataset, combined with the high number of variables and parameters required for the 3D description of the canopy architecture mainly explain why the space of canopy realization is generally poorly sampled, resulting into possibly less robust PAI or GAI estimates.

The objective of this study is to evaluate the retrieval performances from top of canopy reflectance observations of the different xAI (PAI, LAI, GLAI, GAI and GAI_{eff}) state variables of interest. To circumvent the influence of instrument difference and associated measurement errors, the retrieval performances were evaluated with RTM simulations over realistic 3D wheat and maize scenes. To mimic satellite observations using RTM simulations, SENTINEL-2 satellite data which is widely applied in recent crop monitoring applications (Segarra et al. 2020) was selected as an example. We consider a range of phenological stages for wheat and maize crops. We compared the performances of several retrieval methods including VIs combined with a semi-empirical model, and a machine learning based RTM inversion approach using the raw reflectance as inputs and trained with 1D or 3D RTM simulations.

2 Material and methods

We present here how the in-silico experiment was conducted to evaluate the retrieval performances of the several xAI state variables. Realistic 3D wheat and maize scenes (section 2.1 and 2.2) were first combined with 3D RTM simulations (section 2.3) to build a 3D reflectance dataset which was then split into training (70%) and validation (30%). The simulations corresponding to the same training scenes were also conducted with a 1D RTM to train the 1D approach (section 2.4). We then describe the retrieval methods including a neural network machine learning RTM inversion using the raw reflectance as inputs and trained either on the 1D or 3D simulations, and a VIs based approach based on a semi-empirical model (section 2.5). Finally, we present the metrics (section 2.6) that were used to evaluate the retrieval performances of the several state variables and approaches over the 3D reference validation dataset.

2.1 The 3D canopy architecture models

We selected two species characterized by different architectures: (1) wheat with small spacing between rows and plants, and (2) maize with taller plants, larger row, and plant spacing. Wheat canopies shows a clear row structure at early stages, its structure becomes similar to a turbid medium later in the vegetation cycle. Maize canopy is characterized by a row structure that persists up to the latest stages. Leaf inclination varies differently during the growth cycle for both species.

The 3D ADEL-Wheat model (Fournier et al. 2003) was selected to simulate the time course of the 3D architectural growth of wheat. It is an up-to-date model calibrated over a range of experimental conditions (Abichou et al. 2013), where leaf undulation and curvature are considered. For maize, we used the 3D model created by López-Lozano et al. (2007) where plants are described by simple geometric shapes (triangles for leaves and pyramids for stems), Even though this model does not account for leaf undulation and curvature, maize canopies are much better represented than when using a turbid medium model (Casa et al. 2010). As little knowledge is available on ear and flowers optical properties, both wheat and maize were simulated from emergence to the last stage before earing (wheat) or male flowering (maize). For both species, the fraction of senescent leaves appears marginal during this first part of the growth cycle. In such conditions, PAI ≈ GAI and LAI ≈ GLAI. The thermal time (°Cd) is used to drive the wheat and maize development (Hallett and Jones 1993). It corresponds to the accumulated average daily air temperature since emergence.

For each species, 729 canopies were generated according to the variables listed in Table 1. The range of values considered for the input variables were derived from previous experiments (Abichou et al. 2013; López-Lozano et al. 2007; Liu et al. 2017). Each input variable was equally distributed between its minimum and maximum values (Table 1). Five development stages evenly distributed from 100°Cd to 900°Cd for wheat, and from 150°Cd to 950°Cd for maize. The LAI, GLAI, PAI and GAI were calculated from the corresponding area of mock-ups. For LAI, the area of both green and senescent leaves were considered. For PAI, all elements including leaves and stems independently from their colour were considered, while only the area of green parts were considered for GAI. Since around 40% canopies had a GAI smaller than 1.0, 89 canopies with GAI<1 were randomly eliminated from the wheat and maize canopies to avoid some oversampling of low GAI values. Therefore, 640 square scenes of 4.5m side for both wheat and maize were used for the 3D simulations. A typical 3D scene of wheat and maize canopy simulated with ADEL-Wheat and 3D maize models is shown in Figure 1.

Table 1 Parameters of ADEL-Wheat and 3D maize model used in this study.

	Variables		Unit	Min	Typical	Max	Steps
ADEL-Wheat	D	Plant density	plants/m^2	150	250	350	3
	N_{tiller}	Number of tillers per plant	-		3		1
	$N_{leaf.main}$	Number of leaves on the main stem	-		11		1
	TT_{phy}	Phyllochron	°Cd	80	100	120	3
	L_{lamina}	Length of lamina one	cm	8	12	16	3
	Ang_{shift}	Rotation of leaf basal inclination	°	-30	0	30	3
	Ang_{tiller}	Inclination of the base of the tiller	°		20		1
3D	D	Plant density	plants/m^2		9		1
	d_{rows}	Distance between rows	m	0.6	0.7	0.8	3
	N_{max}	Maximum number of leaves per plant	-	18	20	22	3

	TT_{phy}	Phyllochron	°Cd	50			1
	S_{max}	Maximum leaf area per plant	m^2	0.5	0.75	0.75	3
	H_{max}	Maximum plant height	m	2			1
	Θ_{max}	Inclination of largest leaf	°	30	50	60	3

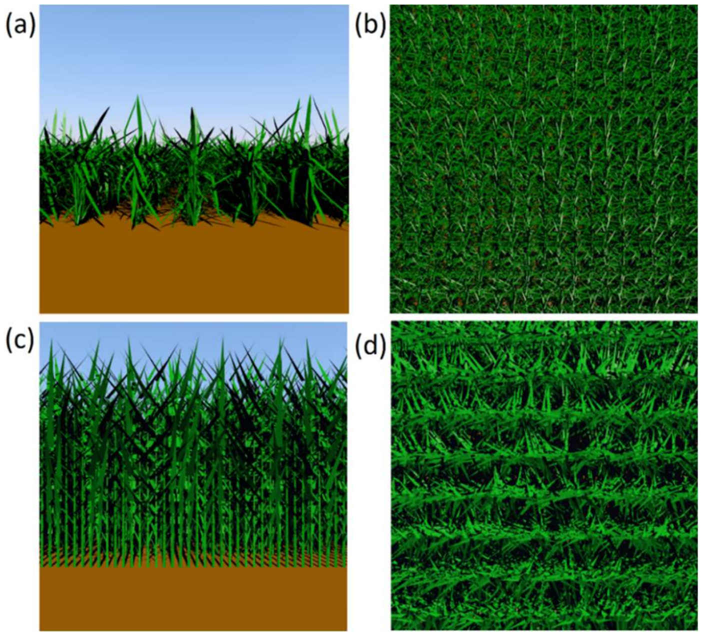

Figure 1 Typical 3D scenes of wheat ((a) front view; (b) top view) and maize ((c) front view; (d) top view) canopy simulated with ADEL-Wheat (LAI=2.26, GAI=2.34, GAI_{eff} I=2.15, PAI=2.56) and 3D maize models. (LAI=4.78, GAI=6.51, GAI_{eff} =4.12, PAI=6.51)

2.2 GAI_{eff} computation

GAI_{eff} was defined consistently with the output of indirect ground measurement methods using hemispherical photography (Weiss et al. 2004). GAI_{eff} was therefore computed from Welles and Norman (1991) which corresponds to a close approximation of Miller's formula (Miller 1967) applied to the green fraction. It relates GAI to the directional green fraction, $GF(\theta)$, assuming that the leaves are randomly distributed in the canopy volume:

$$GAI_{eff} = 2\int_0^{\pi/2} -\ln\big(1 - GF(\theta)\big)\, cos\theta sin\theta \, d\theta \qquad (1)$$

Where θ is the view zenith angle. The green fraction was thus simulated on each scene with LuxCoreRender for six view zenith angles spanning from 0° to 60° and averaged over all the azimuths. Even though part of the small GAI and GAI_{eff} values were discarded, the low values are still the most represented for the two crops (Figure 2).

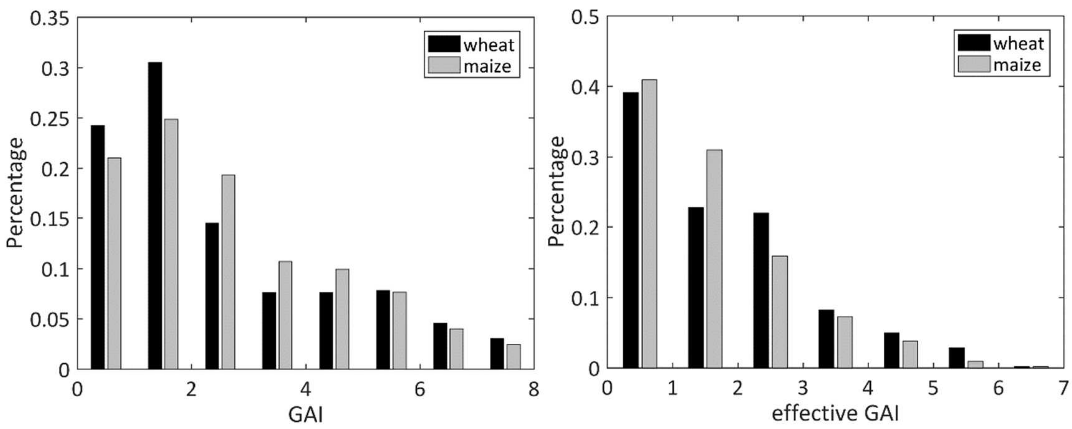

Figure 2 Distribution of GAI (left) and GAI_{eff} (right) of simulated wheat and maize.

2.3 LuxCoreRender reflectance simulations

Canopy reflectance was simulated using the LuxCoreRender 3D render engine (LuxCoreRender 2018) based on the 3D scenes generated by the crop architecture models. LuxCoreRender is an open source software (LuxCoreRender 2018; Pharr et al. 2016), which was validated against a set of state-of-the-art models by Jiang et al. (2020) using the RAMI Online Model Checker (ROMC) (Widlowski et al. 2008) .

The LuxCoreRender ray-tracing integrator was used with 1.36×10^3 samples of light and 16 path depths per pixel to guarantee the accuracy of the rendering of the simulated reflectance. The sun was the only light source with no adjacency contributions nor diffuse incoming radiation. The bidirectional reflectance factor was computed as the ratio of reflected photons in the view direction to those reflected by a perfect lambertian scatterer placed horizontally under the same illumination conditions. Finally, to minimize possible border effects, the 4.5m square scenes were replicated three times on each side to be large enough compared to the footprint of the camera.

Since reflectance simulation with LuxCoreRender is time consuming because of the ray-tracing process, we used the method proposed by Jiang et al. (2020) to speed up the computations of LuxCoreRender: for a given canopy structure and observational configuration, the method allows to accurately compute canopy reflectance for any soil reflectance and any leaf properties (wavelength and biochemical composition) by simulating canopy reflectance for two contrasted backgrounds and six value of the absorption coefficient of the leaf that drives leaf reflectance and transmittance.

Five typical soil spectra with a variability in soil brightness (B_s) were selected to represent a large range of soil background, assumed flat and lambertian (Table 2). Leaves were also assumed lambertian and characterized by their reflectance and transmittance. Stems were characterized by the same reflectance as the leaf with no transmittance. Their optical properties were simulated using the PROSPECT3 model (Baret and Fourty 1997; Jacquemoud and Baret 1990) by considering the contents of four main absorbing element: chlorophyllian pigments (C_{abc}), dry matter (C_{dm}), water (C_w) and brown pigments (C_{bp}). Their distribution laws were defined similarly to Li et al (2015), based on a full factorial experimental plan to sample more evenly the space of canopy realization (Table 2).

We selected six SENTINEL-2A bands in the visible, red-edge, and near infrared domains characterized by the following central wavelengths: 450 nm, 560 nm, 665 nm, 705 nm, 740 nm and 865 nm. For each band, the reflectance was spectrally integrated to take into account the SENTINEL-2A spectral response function.

For each of the 640 scenes considered for each crop (Table 1), the camera was set at a nadir (View Zenith Angle, VZA=0°) corresponding to the most common observational configuration for decametric satellites such as SENTINEL-2. The sun position varied by considering eight Sun Zenith Angles (SZA) and four Sun Azimuth Angles (SAA) defined relatively to the row orientation (Table 2). Note that the row orientation is here linked to the sun azimuthal direction which is made possible because of the nadir view direction.

The 640 scenes were evenly divided into 18 classes according to the value of GAI and the averaged leaf angle (ALA). Finally, for each of the 20 illumination directions considered, a total of 18×5×5×5×3×5=33750 simulations were computed (Table 2). The simulated cases were randomly split into 70% used for the training database and 30% used to validate the retrieval performances of the several state variables and retrieval methods.

Table 2 Distribution of input variables used to generate canopy reflectance with 3D RTM simulations. The column Nb_Class corresponds to the number of levels used for the full factorial experiment design. VZA, SZA, SAA correspond to view zenith angle, sun zenith angle and sun azimuth angle. C_{ab}, C_{dm}, C_w_Rel and B_s represent the chlorophyll content, the dry matter content, the relative water content and soil brightness.

		Input variable	Minimum	Maximum	Mode	Std	Nb_Class	Law
	Observation geometry	VZA(°)	0					
		SZA(°)	20, 35, 50, 65					
		SAA(°)	0, 25, 45, 67, 90					
(Jiang et al. 2020; Koetz et al. 2005; Li et al. 2015)	Leaf optical properties	Refractive Index n	1.4					
		Mesophyll, N	1.5					
		C_{ab}(μg.cm^{-2})	20	90	45	30	5	Gauss
		C_{dm}(g.cm^{-2})	0.003	0.011	0.005	0.005	5	Gauss
		C_w_Rel	0.6	0.85	0.75	0.08	5	Uniform
		C_{bp}	0.0	2.0	0.0	0.3	3	Gauss
	Soil background	B_s	0.5	3.5	1.2	2.0	5	Gauss

2.4 1D PROSAIL simulations

The PROSAIL model (Baret et al. 1992) was generated from the combination of the PROSPECT leaf optical properties model (Jacquemoud and Baret 1990) and the SAIL (Scattering by Arbitrary Inclined Leaves) canopy reflectance model (Verhoef 1984) which assumes the canopy as a turbid medium, i.e. homogeneous infinitely extended horizontal layer of infinitely small leaves randomly distributed. A hotspot parameter was introduced by Kuusk (1985) to account for the fact that leaves have finite dimensions. PROSAIL has been widely used to estimate canopy biophysical and structural variables for applications at different scales (Jacquemoud et al. 2009).

We used the same input variables for PROSPECT and soil background (Table 2) and generated canopy structure variables consistent with those used previously for the 3D models (Table 3). A total of 3×6×5×5×5×3×5=33750 cases were simulated for both wheat and maize. A total of 70% of the simulated cases were randomly selected to match what was done for the 3D training database.

Table 3 Distribution of input variables used to generate the learning database with PROSAIL model.

	Input variable	Minimum	Maximum	Mean	Std	Class	Law
Canopy structure	GAI	0.0	8.0	2.0	3.0	6	Gauss
	ALA (°)	30	70	45	30	3	Gauss
	hotspot	0.1	0.5	0.2	0.5	1	Gauss

2.5 Retrieval methods

2.5.1 Model inversion using neural networks

For each variable, based on the architecture defined by Li et al. (2015), two back-propagation NNs were trained, one using 3D LuxCoreRender and the other one using 1D PROSAIL simulations. This technique was applied operationally to derive kilometric resolution (Baret et al. 2007) or decametric biophysical products (Delloye et al. 2018; Li et al. 2015; Verrelst et al. 2018; Weiss et al. 2002).

For the 3D RTM inversion, the inputs of NN were the canopy reflectance in the six selected SENTINEL-2A bands simulated from 3D model and the associated geometrical configurations including the cosine of SZA and the cosine of relative azimuth angle between SAA and the row direction. The considered outputs were either LAI, GAI or GAI_{eff}. For the 1D PROSAIL inversion, the inputs of the NN were the PROSAIL simulated canopy reflectance in the six selected SENTINEL-2A bands and the cosine of SZA. The corresponding outputs were GAI that indeed equals LAI since no other elements than the green leaves were considered in such a model, and GAI_{eff} that is in agreement with the 1D turbid medium assumption.

2.5.2 VI based empirical retrieval

Many vegetation indices based on the combination of a few spectral bands have been developed to retrieve variables related to the plant photosynthetic activity, such as GAI, fAPAR, and chlorophyll content (Myneni et al. 1995). We selected three vegetation indices among those proposed in the literature (Henrich et al. 2009): the Normalized Difference Vegetation Index (NDVI) (Rouse et al. 1974) which is the most widely used, the optimized Soil-Adjusted Vegetation Index (OSAVI) (Rondeaux et al. 1996) which was designed to minimize the effect from the soil background, and finally, the modified triangular vegetation index (MTVI2) which was found less sensitive to the saturation effect and thus provides more accurate estimates of high GAI values while reducing the influence of the soil background (Haboudane et al. 2004).

$$NDVI = \frac{\rho_{NIR}-\rho_{red}}{\rho_{NIR}+\rho_{red}} \tag{2}$$

$$OSAVI = \frac{\rho_{NIR}-\rho_{red}}{\rho_{NIR}+\rho_{red}+0.16} \tag{3}$$

$$MTVI2 = 1.5\frac{1.2(\rho_{NIR}-\rho_{red})-2.5(\rho_{red}-\rho_{green})}{\sqrt{(2\rho_{NIR}+1)^2-(6\rho_{NIR}-5\sqrt{\rho_{red}})-0.5}} \tag{4}$$

To relate VIs to different definitions of LAI, the modified version of Beer's Law describing VI as an exponential function of the foliage amount F (Broge and Mortensen 2002; Weiss et al. 2002) was selected:

$$VI = VI_\infty + \left(VI_g - VI_\infty\right)exp^{K_{VI}\cdot xAI} \tag{5}$$

where xAI refers either to LAI, GAI, or GAI_{eff}. VI_∞ represents the VI value for a very dense canopy ($xAI \rightarrow \propto$) and VI_g represents the bare soil value ($xAI = 0$) of VI; K_{VI} is equivalent to the extinction coefficient in the Beer Law. For each case, parameters $[VI_\infty,\ VI_g,\ K_{VI}]$ were fitted based on Eq.5 with VIs (NDVI, OSAVI, MTVI2) and LAI (or GAI, GAI) calculated from the training database which were generated to train the 3D RTM neural networks.

2.6 Performance metrics

The validation dataset generated from 3D simulation was used to evaluate the inversion results from NNs trained with 1D or 3D simulations.The root mean square error (RMSE) and the coefficient of determination (R^2) are used to evaluate the agreement between the original F value and the estimated one.

3 Results

3.1 Contribution of the stems and senescent parts to PAI

For the early stages (thermal time lower than 300°Cd), the stem area is negligible. After this period, the stem area is increasing and can have a PAI between 1 or 2 (Figure 3) representing almost one fourth of the total plant area. The maize simulated canopies have greater PAI than the wheat ones. The several scenes simulated by ADEL-Wheat and the 3D maize architecture models show a marginal fraction of senescent elements as already pointed out (Figure 3). Further, the senescent elements are mainly located at the bottom of the canopy, with a marginal contribution to canopy reflectance (Figure S1 provides an example of wheat canopy reflectance with or without senescent leaves in red and NIR). As a consequence, LAI≈GLAI and PAI≈GAI, thus GLAI and PAI will not be explicitly considered in the following of this study.

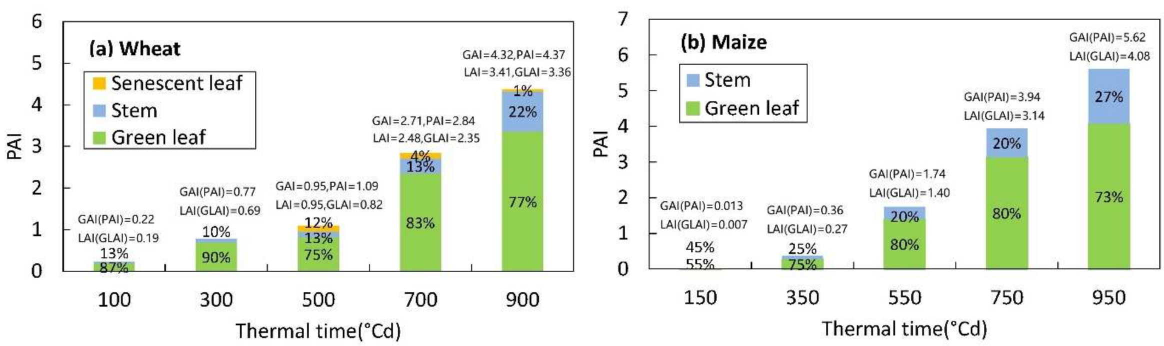

Figure 3 Plant Area Index and the corresponding proportion of green leaves (green), senescent leaves (yellow) and stems (blue) of typical wheat (a) and maize (b) canopies during the vegetative stages.

3.2 Impact of canopy structure assumptions on reflectance

We investigated the contribution of the stems to canopy reflectance as well as the role of the spatial distribution of the elements. One 3D scene of wheat and maize were randomly selected from the 3D wheat and maize architecture models (Section 2.1). The statistics of PAI, LAI, GLAI and GAI of those scenes were described in Figure 3. Based on the LuxCoreRender reflectance simulations (Section 2.3), we simulated the 3D scenes canopy reflectance in the Red (665nm) and NIR (865nm) bands. For the sake of simplicity, constant optical properties of the canopy elements and soil background were used (Table 4). The view direction was set at nadir with SZA=45° and SAA= [0°, 45°, 90°].

Table 4 Optical properties of the different elements (leaves, stem, and soil background) used to analyze the impact of wheat and maize canopy architecture assumptions on reflectance in the red and NIR domain.

	Reflectance		Transmittance	
	Red	NIR	Red	NIR
Green leaf	0.063	0.463	0.018	0.522
Stem	0.063	0.463	0.000	0.000
Senescent leaf	0.347	0.474	0.287	0.432
Soil	0.140	0.191	-	-

Results show that the stems have almost no influence on canopy reflectance in the red domain (Figure 4a and Figure 4c) especially when the soil contribution is the highest (SAA=0°). This is explained by the low value of leaf and stem reflectance and transmittance. Conversely, in the NIR domain, stems showed significant impact on canopy reflectance, particularly for the later stages when the contribution of stems to GAI increases (Figure 4b and Figure 4d). The decrease of canopy reflectance due to the stems in the NIR is mainly explained by the strong stem absorption (null transmittance) that reduces the multiple scattering.

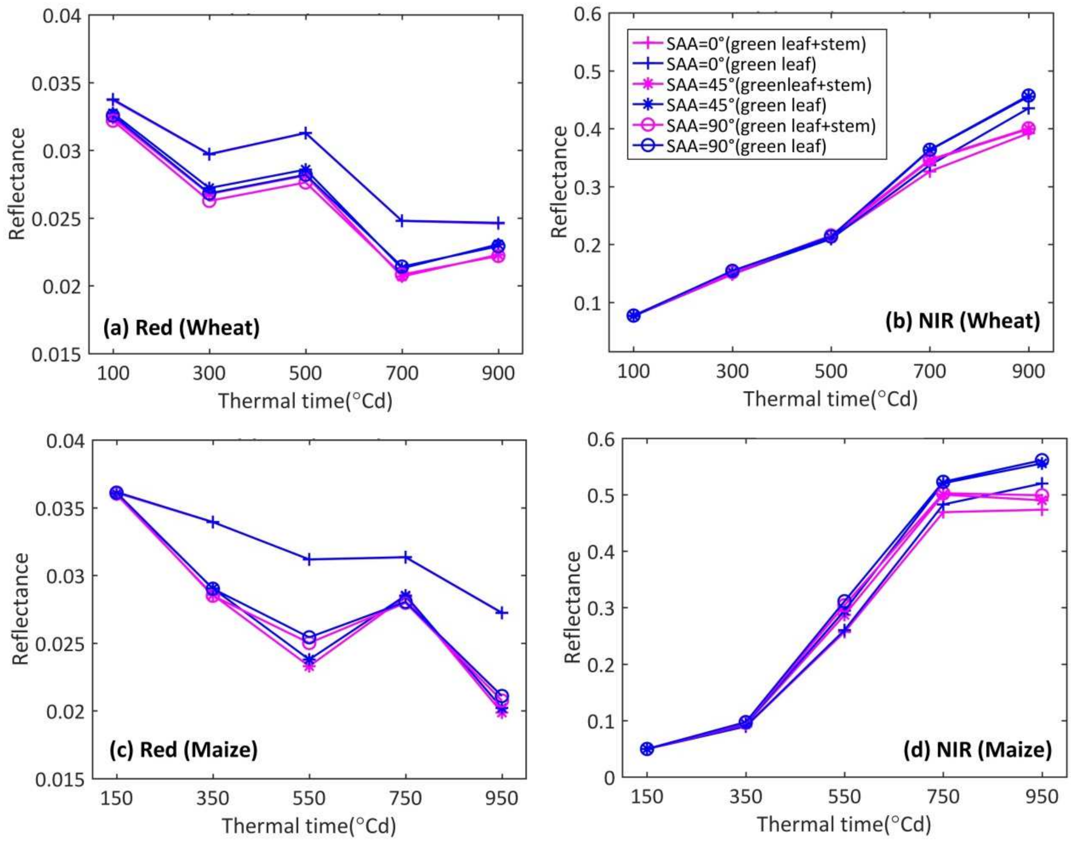

Figure 4 Comparison of canopy nadir reflectance (3D structure) between canopy with leaves and stems (red) and canopy with only leaves (blue) in red (left) and NIR (right) for wheat (top) and maize (bottom) for three sun azimuth angles values SAA = 0° (+), 45° (*) and 90° (○) and a sun zenith angle at 45°.

We then simulated a turbid medium version of each scene by keeping the same canopy elements with their corresponding optical properties and original orientation, and distributed them randomly in the canopy volume. This allowed performing a fair comparison between a random medium (1D) and the actual 3D crop architecture. Because of this random distribution of the elements in the 1D canopy structure description of wheat and maize (Figure 5), reflectance is independent from the sun azimuthal position. Conversely, canopy reflectance of the 3D realistic canopy architecture shows significant variations with sun azimuth, especially when the sun is parallel to the row direction and under its nominal zenith angle (SZA=45°).

In the NIR, the 1D canopy always shows a higher crop reflectance than the 3D one (Figure 5b and Figure 5d). This is mainly due to a higher probability for a photon to interact with a leaf in the absence of clumping (Duthoit et al. 2008). This boosts multiple scattering and lowers the soil contribution, the soil being less reflective in the NIR than the leaves (Table 4). Conversely in the red domain, the soil is more reflective in the red as compared to leaves (Table 4). When the sun is parallel to the row direction (SAA=0°), the higher proportion of soil illuminated between the rows in the 3D description explains that canopy reflectance is higher than that of the 1D description (Figure 5a and Figure 5c). When canopy develops, the difference in reflectance between 1D and 3D assumptions increases for maize while remaining almost constant for wheat. This demonstrates that, conversely to maize, for the latest stages, the structure of the wheat canopy becomes closer to a turbid medium, with a decreasing row effect.

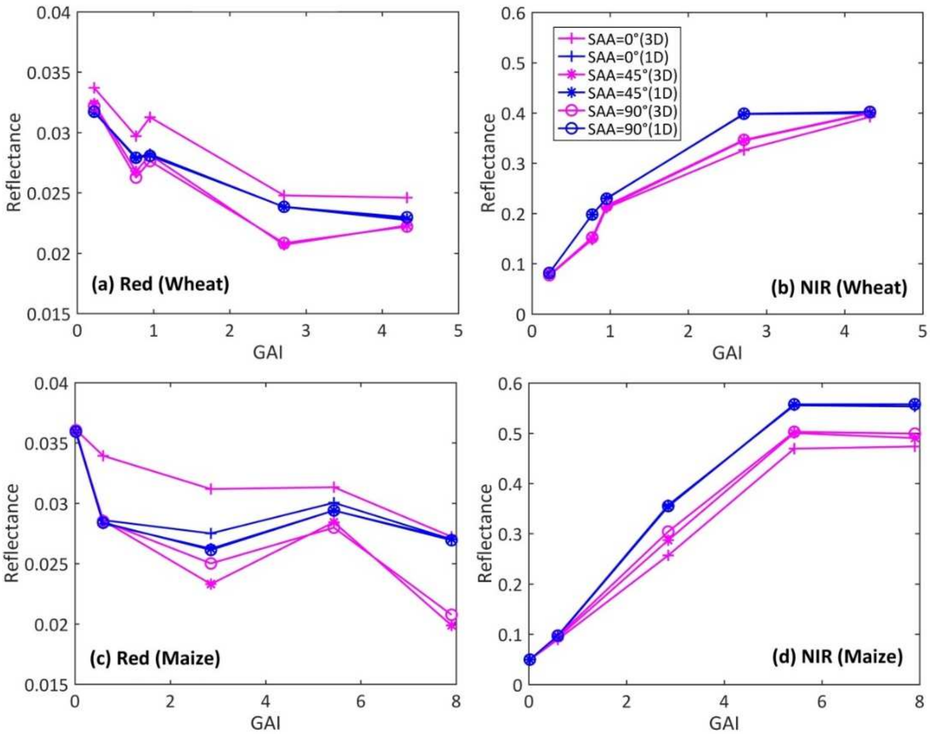

Figure 5 Comparison of canopy nadir reflectance between turbid medium assumption (magenta) and 3D realistic structure (blue) in red (left) and NIR (right) for wheat (top) and maize (bottom) for three sun azimuth angles values SAA = 0° (+), 45° (*) and 90° (○)and a sun zenith angle at 45°.

3.3 GAI_{eff} is better estimated than LAI and GAI

NN were trained on the 3D wheat or maize canopies to estimate either LAI, GAI or GAI_{eff}. The retrieval performances were evaluated on the 3D simulated validation dataset that was not used during the training process. Results showed that LAI and GAI are estimated with similar performances in terms of R^2 (Figure 6). However, RMSE values for GAI are slightly larger mainly because of the larger range of variation of GAI as compared to LAI that does not include the area of green stems. Slight systematic underestimation is observed for the high LAI and GAI values, which is due to the combined effect of reflectance saturation (Price and Bausch 1995) and the fact that, conversely to Li et al (2015), the training dataset is limited by the fewer representative cases of LAI or GAI above 6 (Figure 6). The estimation of GAI_{eff} showed the best performance with the highest R^2 and the smallest RMSE (RMSE = 0.33, R^2 = 0.95 for wheat and RMSE = 0.43, R^2 = 0.90 for maize). Here again, the smaller values of RMSE are partly explained by the smaller range of variation of the GAI_{eff} as compared to LAI and GAI. The scattering around the 1:1 line slightly increases with LAI, GAI or GAI_{eff} because of the decreasing sensitivity of reflectance to variation in the amount of green area as already observed in Figure 4 and Figure 5. Therefore, GAI_{eff} appears as a pertinent variable when using reflectance observations over typical crops. Furthermore, it offers the advantage of being more directly comparable to estimates of the GAI_{eff} derived from indirect ground measurements techniques (Jonckheere et al. 2004). This will allow to validate GAI_{eff} values estimated from remote sensing without explicitly handling the complex problem of accounting for the leaf clumping (Leblanc and Fournier 2014).

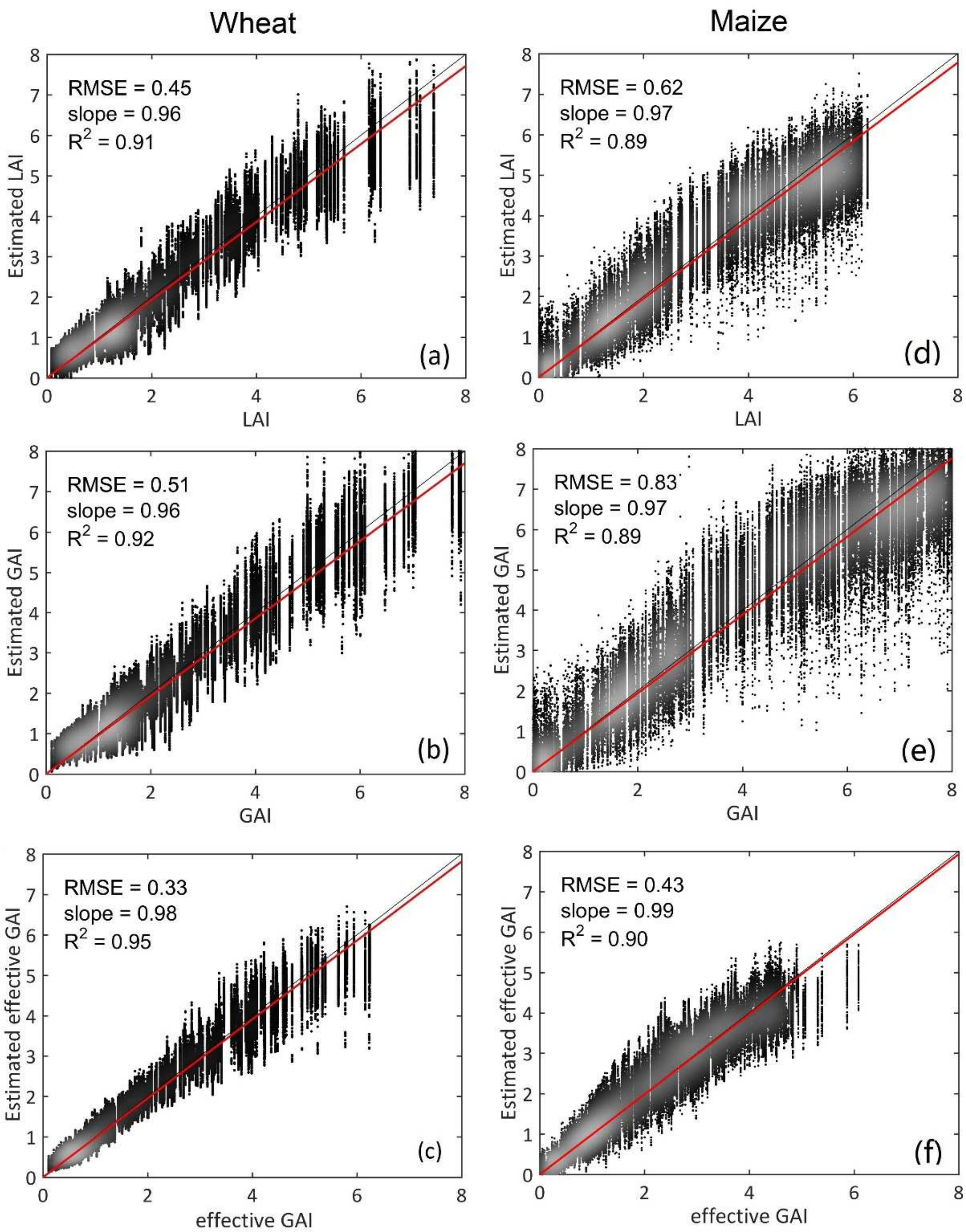

Figure 6 Scatter plots between state variables estimated from neural networks trained over 3D model simulations and wheat LAI (a), wheat GAI (b), wheat GAI_{eff} (c), maize LAI (d) , maize GAI (e), and maize GAI_{eff} (f). The lighter color increases with the point density. The black line corresponds to the 1:1 line. The red line is the best linear fit with no intercept.

3.4 Performances of GAI_{eff} estimates are almost insensitive to the sun position

Retrieval of GAI_{eff} from ground measurements of the green fraction exploits all the directions of the hemisphere (Eq. 1). Conversely, canopy reflectance depends on the sun and view directions which are explicitly used as inputs into the retrieval process. We therefore investigated here the possible residual impact of the sun position on the retrieval performances of GAI_{eff} under near nadir viewing direction that corresponds to the most common observational configuration for decametric satellites such as SENTINEL-2. Results show that GAI_{eff} estimation performances are little sensitive to the sun position (Figure 7), with RMSE between 0.3 and 0.4. However, a slight degradation of GAI_{eff} retrieval performances is observed when SZA increases. This may be explained by the larger optical depth in the canopy for the more inclined illumination directions that makes canopy reflectance less sensitive to the elements placed at the bottom of the canopy. The change in SAA marginally impacts performances for wheat, in agreement with the small row effect and closeness to the turbid medium assumption. Nevertheless, some small effect is observed for SZA=65°, where slightly better performances are observed when the sun is parallel to the rows. This may be due to the enhanced reflectance sensitive to changes in GAI in the inter-row spacing for the higher GAI values while saturation occurs earlier on the row. The same is observed for maize (Figure 7). However, significant degradation of performances are observed for maize for SZA<40° and sun directions close to that of the row. This may be due to the combined effect of the higher sensitivity to the background properties when the soil is well illuminated, and an earlier saturation of reflectance to changes in GAI on the row.

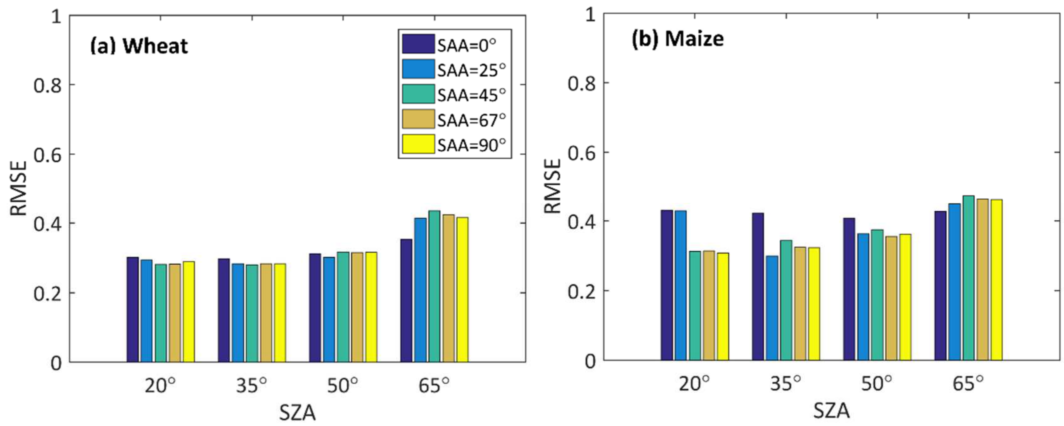

Figure 7 RMSE between GAI_{eff} and estimated GAI_{eff} from NN trained with 3D datasets for wheat (a) and maize (b). Results are evaluated using the validation dataset for several sun azimuth angles (SAA) and sun zenith angles (SZA).

3.5 3D structure description improves estimates of GAI_{eff} as compared to a 1D description

The same GAI_{eff} value may correspond to a range of canopy structure associated to a range of radiometric response. We therefore compared the performances of GAI_{eff} estimation using either a 1D radiative transfer model such as PROSAIL, or the realistic 3D models of wheat or maize. Results show that for both wheat and maize, accounting for the 3D structure description (Figure 6c and Figure 6f) provides more accurate estimates of GAI_{eff} than the turbid medium assumption (Figure 8). Conversely to the GAI_{eff} derived from NN trained with the 3D model, the 1D model inversion resulted in a systematic underestimation for both crops when GAI_{eff} is higher than 4. For GAI_{eff} lower than 4, the estimated GAI_{eff} from PROSAIL model shows good agreement with GAI_{eff} for wheat (Figure 8a), while more outliers are observed for maize. Similar results are observed by Duveiller et al. (2011) and Camacho et al. (2017) who compared indirect GAI_{eff} measurements with estimates from NN trained on PROSAIL.

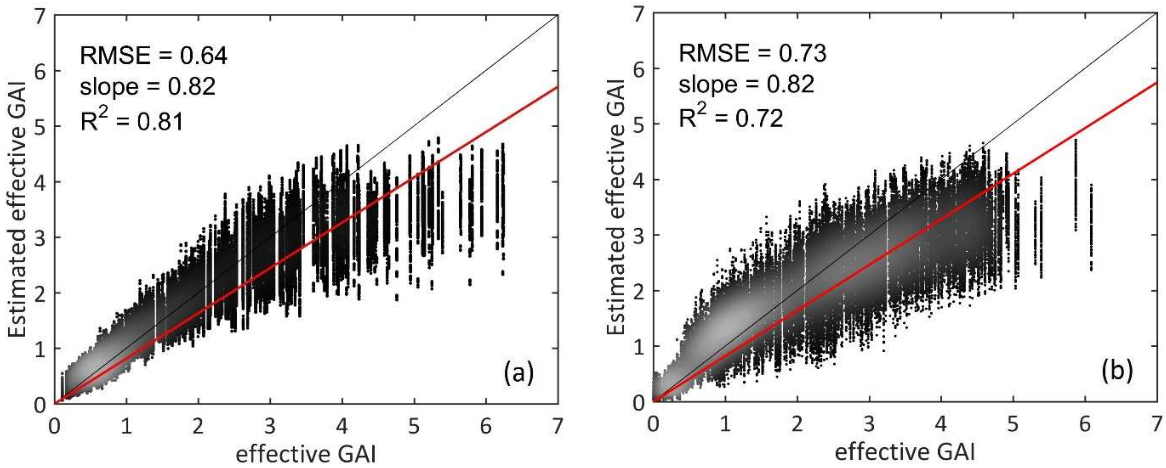

Figure 8 Scatter plots between estimated GAI_{eff} from NN trained over PROSAIL model simulations and GAI_{eff} for (a) wheat and (b) maize. The grey level intensity increases with the density of points. The black line corresponds to the 1:1 line. The red line is the best linear fit with no intercept.

3.6 Using raw reflectance values and machine learning performs better than vegetation indices and a semi-empirical model

The parameters of the empirical model (Eq. 5) describing the relationship between VIs and GAI_{eff} were fitted over the training database made of 3D model simulations. Since Eq. 5 does not account explicitly for the illumination direction, parameters $[VI_{\infty},\ VI_g,\ K_{VI}]$ were tuned for each sun zenith and azimuth angles, and when considering all the sun angles together. The values of K_{VI} with different sun directions were showed in Table S1. Results showed better GAI_{eff} estimates (higher R^2) for most of the sun angles when the parameters $[VI_{\infty},\ VI_g,\ K_{VI}]$ are tuned for each illumination direction (Table 5). The R^2 are significantly lower for maize as compared to wheat. OSAVI and MTVI2 are performing better than NDVI since they were designed to be less sensitive to the soil background and the canopy structure (Liu et al. 2012; Nguy-Robertson et al. 2012). Highest R^2 are observed when the sun is parallel to the rows (SAA=0°) similarly to what was observed in Figure 7 when using the raw reflectances from 3D simulations and a machine learning inversion.

Table 5. Determination coefficients (R^2) associated to the goodness of fit of Eq. 5 between VIs (NDVI, OSAVI and MTVI2) observed on the training database made of 3D model simulations. The several sun directions [SZA, SAA] are either considered separately or grouped together. Red color indicates the poorest performances while green corresponds to the best ones.

	SZA / SAA	NDVI				OSAVI				MTVI2			
		20°	35°	50°	65°	20°	35°	50°	65°	20°	35°	50°	65°
Wheat	0°	0.68	0.69	0.68	0.67	0.73	0.74	0.74	0.7	0.83	0.84	0.83	0.79
	25°	0.69	0.69	0.69	0.36	0.74	0.75	0.75	0.71	0.84	0.81	0.73	0.58
	45°	0.7	0.7	0.58	0.26	0.76	0.74	0.74	0.66	0.84	0.74	0.66	0.64
	67°	0.69	0.68	0.53	0.26	0.76	0.76	0.75	0.66	0.83	0.73	0.64	0.64
	90°	0.7	0.68	0.53	0.27	0.75	0.76	0.75	0.66	0.82	0.72	0.65	0.62
	All angles	0.54				0.7				0.65			
Maize	0°	0.55	0.56	0.54	0.46	0.55	0.56	0.58	0.61	0.66	0.68	0.69	0.66
	25°	0.63	0.54	0.18	0.11	0.62	0.66	0.53	0.16	0.67	0.64	0.62	0.48
	45°	0.59	0.41	0.15	0.11	0.66	0.6	0.48	0.1	0.65	0.57	0.61	0.43
	67°	0.52	0.42	0.15	0.1	0.63	0.59	0.47	0.1	0.61	0.59	0.6	0.42
	90°	0.5	0.43	0.18	0.1	0.64	0.59	0.47	0.14	0.6	0.59	0.59	0.46
	All angles	0.21				0.46				0.42			

Eq. 5 fitted for each illumination direction over the 3D training dataset was then evaluated over the 3D validation database to estimate GAI_{eff}. For both wheat and maize crops, OSAVI appears to perform slightly better than MTVI2, and significantly better than NDVI (Table 6). However, using the raw reflectances from 3D model simulations as input to the NN for GAI_{eff} estimation outperforms VIs with RMSE values divided by almost a factor of two (Table 6). The higher degree of flexibility of the model inversion approach based on machine-learning explains most of these improved performances. Indeed, about 50 coefficients were tuned in case of the NN while only three are fitted in Eq. 5. for the VI based approach. Furthermore, VIs are using only two to three wavebands as compared to the six wavebands used in the machine learning based inversion approach.

Table 6 GAI_{eff} retrieval performances using VIs (NDVI, OSAVI and MTVI2), or neural networks trained on raw reflectances from 3D model simulations. Colors are coded according to the RMSE or R^2 values from best (green) to worst (red).

	Wheat		Maize	
	RMSE	R^2	RMSE	R^2
NDVI	0.95	0.54	1.21	0.21
OSAVI	0.77	0.70	1.00	0.46
MTVI2	0.83	0.65	1.02	0.42
Raw reflectances	0.33	0.95	0.43	0.90

4 Discussion

In this study, we investigated the several ways to characterize the area of canopy elements from remote sensing observations based on 3D simulation. The question is complex since at least two aspects should be tackled concurrently: First, among PAI, LAI, GLAI, GAI and GAI_{eff}, which quantity is best estimated from reflectance data? Second, is this quantity useful for given applications? Our simulations conducted over wheat and maize crops clearly demonstrated that the GAI_{eff} is the quantity that is best estimated from nadir reflectance observations in 6 bands corresponding to a standard configuration of decametric resolution satellite observations as provided since 2015 by SENTINEL-2. However, in this study, the amount of senescent elements was marginal, which implies that PAI≈GAI and LAI≈GLAI. Further simulations should be conducted for later stages where the senescent elements are increasingly present. The results we obtained over two major crops should be extended to other vegetation types to verify the robustness and the validity of our results. The second aspect, i.e. the pertinence of the GAI_{eff} for applications, requires more attention. Indeed, considering all the green vegetation elements (GAI) that are potentially active appears well suited when monitoring the capacity of the crop to grow, or to quantify its past growth. However, GAI_{eff} is better suited to quantify the light interception efficiency according to the proposed definition based on the directional green fraction. Additionally, this offers the advantage to get a definition that is fully consistent with indirect ground methods that can be used for the validation. It can also be used for the calibration of machine learning algorithms over ground experiments if empirical approaches such as those conducted by Camacho et al. (2017) are further investigated. Ultimately, the use of GAI_{eff} that is clearly defined and more robustly estimated, may also help when integrating remote sensing observations into crop growth models for which canopy structure is generally described in a very simple way.

The next question that we investigated was related to the best canopy architecture description required to get accurate estimates of the targeted GAI_{eff} variable from reflectance observations. We thus compared realistic 3D canopy architecture description with the 1D counterpart that is consistent with the turbid medium nature used to define the 'effective' GAI. We used a neural network machine learning algorithm to invert both the 1D and 3D models. Results obtained over an independent set of 3D canopy architecture simulations clearly demonstrated the importance of using a realistic 3D canopy architecture description to get reflectance simulations as close as possible to the observed ones.

Finally, we also investigated the best GAI_{eff} retrieval approach by comparing the use of VIs and a semi-empirical model versus the use of raw relectances with a machine learning based RTM inversion. Results clearly demonstrated that VIs have strong limitations due to at least three factors: First, the fact that they are not exploiting the whole spectral information available since they generally use two to three bands as compared to the six ones that were used in the radiative transfer model inversion; Second, the simple combination of bands used to compute VIs results into a loss in information as compared to using the original reflectance wavebands as inputs in the retrieval algorithm; Third, the semi-empirical model relating the GAI_{eff} to VIs is using only three parameters to account for the variability in canopy architecture, leaf and soil properties, even if the illumination conditions are accounted for by adjusting the three parameters for each conditions.

5 Conclusion

In this study, canopy reflectance and the corresponding variables including LAI, PAI, GAI and GAI_{eff} were first calculated using a 3D RTM applied to 3D wheat and maize architecture models. Different inversion methods including VIs, 1D RTM PROSAIL and 3D RTM LuxCoreRender are compared.

Results show that GAI_{eff} is best estimated from remote sensing observations and is better suited with indirect ground measurements at the decametric scale. The outcomes also indicate that the best GAI_{eff} retrieval approach would be to train machine learning algorithms using a training database where accurate GAI_{eff} values are paired with accurate corresponding reflectance values. The 3D model simulations as completed in this study is a possible solution that requires the canopy architecture models to be very realistic, and the distribution of their input parameters and variables very well designed to represent the actual ones. However, the retrieval methods based on 3D model simulations presented in this study should be extended to other types of vegetation and then evaluated using actual observations. Alternatively, empirical approaches based on accurate GAI_{eff} values measured from indirect ground methods and on concurrent corresponding canopy reflectance measured by the satellite are very appealing. They need however to sample a large range of canopy state and illumination conditions. This is now possible for decametric resolution, where the ground measurement effort is affordable over decametric pixel size.

Declaration of Competing Interest

The authors declare that they have no known competing financial interests or personal relationships that could have appeared to influence the work reported in this paper.

Acknowledgment

This work was financially supported by the Fundamental Research Funds for the Central Universities (Grant No.2021ZY13), the National Natural Science Foundation of China (Grant No. 42101329), and Open Fund of State Key Laboratory of Remote Sensing Science (Grant No. OFSLRSS202115).

References

Abichou, M., Fournier, C., Dornbusch, T., CHAMBON, C., Baccar, R., Bertheloot, J., Vidal, T., Robert, C., Gouache, D., & Andrieu, B. (2013). Re-parametrisation of Adel-wheat allows reducing the experimental effort to simulate the 3D development of winter wheat. In, *7. International Conference on Functional Structure Plant Models* (p. np). Saariselkä, Finland: Finnish Society of Forest Science

Banskota, A., Serbin, S.P., Wynne, R.H., Thomas, V.A., Falkowski, M.J., Kayastha, N., Gastellu-Etchegorry, J.-P., & Townsend, P.A. (2015). An LUT-based inversion of DART model to estimate forest LAI from hyperspectral data. *IEEE Journal of Selected Topics in Applied Earth Observations and Remote Sensing, 8*, 3147-3160

Baret, F., & Buis, S. (2008). Estimating Canopy Characteristics from Remote Sensing Observations: Review of Methods and Associated Problems. In S. Liang (Ed.), *Advances in Land Remote Sensing* (pp. 173-201): Springer Netherlands

Baret, F., de Solan, B., Lopez-Lozano, R., Ma, K., & Weiss, M. (2010). GAI estimates of row crops from downward looking digital photos taken perpendicular to rows at 57.5 degrees zenith angle: Theoretical considerations based on 3D architecture models and application to wheat crops. *Agricultural and Forest Meteorology, 150*, 1393-1401

Baret, F., & Fourty, T. (1997). Estimation of leaf water content and specific leaf weight from reflectance and transmittance measurements. *Agronomie, 17*, 455-464

Baret, F., Guyot, G., & Major, D.J. (1989). Crop biomass evaluation using radiometric measurements. *Photogrammetria (PRS), 43*, 241-256

Baret, F., Hagolle, O., Geiger, B., Bicheron, P., Miras, B., Huc, M., Berthelot, B., Nino, F., Weiss, M., Samain, O., Roujean, J.L., & Leroy, M. (2007). LAI, fAPAR and fCover CYCLOPES global products derived from VEGETATION: Part 1: Principles of the algorithm. *Remote Sensing of Environment, 110*, 275-286

Baret, F., Jacquemoud, S., Guyot, G., & Leprieur, C. (1992). Modeled analysis of the biophysical nature of spectral shifts and comparison with information content of broad bands. *Remote Sensing of Environment, 41*, 133-142

Berger, M., Moreno, J., Johannessen, J.A., Levelt, P.F., & Hanssen, R.F. (2012). ESA's sentinel missions in support of Earth system science. *Remote Sensing of Environment, 120*, 84-90

Biskup, B., Scharr, H., Schurr, U., & Rascher, U. (2007). A stereo imaging system for measuring structural parameters of plant canopies. *Plant, Cell & Environment, 30*, 1299-1308

Brede, B., Gastellu-Etchegorry, J.-P., Lauret, N., Baret, F., Clevers, J., Verbesselt, J., & Herold, M. (2018). Monitoring Forest Phenology and Leaf Area Index with the Autonomous, Low-Cost Transmittance Sensor PASTiS-57. *Remote Sensing, 10*, 1032

Broge, N.H., & Leblanc, E. (2001). Comparing prediction power and stability of broadband and hyperspectral vegetation indices for estimation of green leaf area index and canopy chlorophyll density. *Remote Sensing of Environment, 76*, 156-172

Broge, N.H., & Mortensen, J.V. (2002). Deriving green crop area index and canopy chlorophyll density of winter wheat from spectral reflectance data. *Remote Sensing of Environment, 81*, 45-57

Camacho-Collados, J., Pilehvar, M.T., Collier, N., & Navigli, R. (2017). Semeval-2017 task 2: Multilingual and cross-lingual semantic word similarity. In, *Proceedings of the 11th International Workshop on Semantic Evaluation (SemEval-2017)* (pp. 15-26)

Campbell, G.S., & Norman, J.M. (1988). The description and measurements of plant canopy structure. In B.M.a.P.G.J.G. Russell (Ed.), *Plant canopies: their growth, form and function* (pp. 1-19): Cambridge University Press

Casa, R., Baret, F., Buis, S., Lopez-Lozano, R., Pascucci, S., Palombo, A., & Jones, H.G. (2010). Estimation of maize canopy properties from remote sensing by inversion of 1-D and 4-D models. *Precision agriculture, 11*, 319-334

Chen, J.M., & Black, T. (1992). Defining leaf area index for non‐flat leaves. *Plant, Cell & Environment, 15*, 421-429

Delloye, C., Weiss, M., & Defourny, P. (2018). Retrieval of the canopy chlorophyll content from Sentinel-2 spectral bands to estimate nitrogen uptake in intensive winter wheat cropping systems. *Remote Sensing of Environment, 216*, 245-261

Demarez, V., Duthoit, S., Baret, F., Weiss, M., & Dedieu, G. (2008). Estimation of leaf area and clumping indexes of crops with hemispherical photographs. *Agricultural and Forest Meteorology, 148*, 644-655

Domingo, F., Sánchez, G., Moro, M., Brenner, A., & Puigdefábregas, J. (1998). Measurement and modelling of rainfall interception by three semi-arid canopies. *Agricultural and Forest meteorology, 91*, 275-292

Duan, S.-B., Li, Z.-L., Wu, H., Tang, B.-H., Ma, L., Zhao, E., & Li, C. (2014). Inversion of the PROSAIL model to estimate leaf area index of maize, potato, and sunflower fields from unmanned aerial vehicle hyperspectral data. *International Journal of Applied Earth Observation and Geoinformation, 26*, 12-20

Duthoit, S., Demarez, V., Gastellu-Etchegorry, J.-P., Martin, E., & Roujean, J.-L. (2008). Assessing the effects of the clumping phenomenon on BRDF of a maize crop based on 3D numerical scenes using DART model. *Agricultural and Forest Meteorology, 148*, 1341-1352

Duveiller, G., Weiss, M., Baret, F., & Defourny, P. (2011). Retrieving wheat Green Area Index during the growing season from optical time series measurements based on neural network radiative transfer inversion. *Remote Sensing of Environment, 115*, 887-896

Fang, H., Liu, W., Li, W., & Wei, S. (2018). Estimation of the directional and whole apparent clumping index (ACI) from indirect optical measurements. *ISPRS Journal of Photogrammetry and Remote Sensing, 144*, 1-13

Fournier, C., Andrieu, B., Ljutovac, S., & Saint-Jean, S. (2003). ADEL-wheat: a 3D architectural model of wheat development. In: Springer Verlag

Gascon, F., Gastellu-Etchegorry, J.-P., Lefevre-Fonollosa, M.-J., & Dufrene, E. (2004). Retrieval of forest biophysical variables by inverting a 3-D radiative transfer model and using high and very high resolution imagery. *International Journal of Remote Sensing, 25*, 5601-5616

Gastellu-Etchegorry, J., Martin, E., & Gascon, F. (2004). DART: a 3D model for simulating satellite images and studying surface radiation budget. *International Journal of Remote Sensing, 25*, 73-96

Gonsamo, A. (2009). *Remote sensing of leaf area index: enhanced retrieval from close-range and remotely sensed optical observations*. University of Helsinki, Department of Geography

González-Sanpedro, M., Le Toan, T., Moreno, J., Kergoat, L., & Rubio, E. (2008). Seasonal variations of leaf area index of agricultural fields retrieved from Landsat data. *Remote Sensing of Environment, 112*, 810-824

Gower, S.T., Kucharik, C.J., & Norman, J.M. (1999). Direct and indirect estimation of leaf area index, fAPAR, and net primary production of terrestrial ecosystems. *Remote Sensing of Environment, 70*, 29-51

Haboudane, D., Miller, J.R., Pattey, E., Zarco-Tejada, P.J., & Strachan, I.B. (2004). Hyperspectral vegetation indices and novel algorithms for predicting green LAI of crop canopies: Modeling and validation in the context of precision agriculture. *Remote Sensing of Environment, 90*, 337-352

Hallett, S.H., & Jones, R.J. (1993). Compilation of an accumulated temperature database for use in an environmental information system. *Agricultural and Forest Meteorology, 63*, 21-34

Henrich, V., Götze, E., Jung, A., Sandow, C., Thürkow, D., & Gläßer, C. (2009). Development of an Online indices-database: motivation, concept and implementation. *EARSeL proceedings, EARSeL, Tel Aviv*

Hernández-Clemente, R., North, P., Hornero, A., & Zarco-Tejada, P. (2017). Assessing the effects of forest health on sun-induced chlorophyll fluorescence using the FluorFLIGHT 3-D radiative transfer model to account for forest structure. *Remote Sensing of Environment, 193*, 165-179

Jacquemoud, S., Bacour, C., Poilve, H., & Frangi, J.-P. (2000). Comparison of four radiative transfer models to simulate plant canopies reflectance: Direct and inverse mode. *Remote Sensing of Environment, 74*, 471-481

Jacquemoud, S., & Baret, F. (1990). PROSPECT : A model of leaf optical properties spectra. *Remote Sensing of Environment, 34*, 75-91

Jacquemoud, S., Verhoef, W., Baret, F., Bacour, C., Zarco-Tejada, P.J., Asner, G.P., François, C., & Ustin, S.L. (2009). PROSPECT + SAIL models: A review of use for vegetation characterization. *Remote Sensing of Environment, 113*, S56-S66

Jiang, J., Weiss, M., Liu, S., Rochdi, N., & Baret, F. (2020). Speeding up 3D radiative transfer simulations: a physically based metamodel of canopy reflectance dependency on wavelength, leaf biochemical composition and soil reflectance. *Remote Sensing of Environment, 237*, 111614

Jonckheere, I., Fleck, S., Nackaerts, K., Muys, B., Coppin, P., Weiss, M., & Baret, F. (2004). Review of methods for in situ leaf area index determination: Part I. Theories, sensors and hemispherical photography. *Agricultural and Forest Meteorology, 121*, 19-35

Koetz, B., Baret, F., Poilvé, H., & Hill, J. (2005). Use of coupled canopy structure dynamic and radiative transfer models to estimate biophysical canopy characteristics. *Remote Sensing of Environment, 95*, 115-124

Kuusk, A. (1985). The hot spot effect on a uniform vegetative cover. *Sov J Remote Sens, 3*, 645-658

López-Lozano, R., Baret, F., Chelle, M., Rochdi, N., & España, M. (2007). Sensitivity of gap fraction to maize architectural characteristics based on 4D model simulations. *Agricultural and Forest Meteorology, 143*, 217-229

Leblanc, S., Chen, J., Fernandes, R., Deering, D.W., & Conley, A. (2005). Methodology comparison for canopy structure parameters extraction from digital hemispherical photography in boreal forests. *Agricultural and Forest Meteorology, 129*, 187-207

Leblanc, S.G., & Fournier, R.A. (2014). Hemispherical photography simulations with an architectural model to assess retrieval of leaf area index. *Agricultural and Forest Meteorology, 194*, 64-76

Li, W., Weiss, M., Waldner, F., Defourny, P., Demarez, V., Morin, D., Hagolle, O., & Baret, F. (2015). A generic algorithm to estimate LAI, FAPAR and FCOVER variables from SPOT4_HRVIR and landsat sensors: evaluation of the consistency and comparison with ground measurements. *Remote Sensing, 7*, 15494-15516

Liang, S. (2004). *Quantitative remote sensing of land surfaces*. (1st ed.). New York, the USA: John Wiley & Sons

Liu, J., Pattey, E., & Jégo, G. (2012). Assessment of vegetation indices for regional crop green LAI estimation from Landsat images over multiple growing seasons. *Remote Sensing of Environment, 123*, 347-358

Liu, S., Baret, F., Abichou, M., Boudon, F., Thomas, S., Zhao, K., Fournier, C., Andrieu, B., Irfan, K., & Hemmerlé, M. (2017). Estimating wheat green area index from ground-based LiDAR measurement using a 3D canopy structure model. *Agricultural and Forest meteorology, 247*, 12-20

Lord, D., Desjardins, R.L., & Dubé, P.A. (1988). Sun-angle effects on the red and near infrared reflectances of five different crop canopies. *Canadian Journal of Remote Sensing, 14*, 46-55

LuxCoreRender (2018). LuxCoreRender Wiki. https://wiki.luxcorerender.org/LuxCoreRender_Wiki. In

Malenovský, Z., Homolová, L., Zurita-Milla, R., Lukeš, P., Kaplan, V., Hanuš, J., Gastellu-Etchegorry, J.-P., & Schaepman, M.E. (2013). Retrieval of spruce leaf chlorophyll content from airborne image data using continuum removal and radiative transfer. *Remote Sensing of Environment, 131*, 85-102

Martello, M., Ferro, N., Bortolini, L., & Morari, F. (2015). Effect of incident rainfall redistribution by maize canopy on soil moisture at the crop row scale. *Water, 7*, 2254-2271

Miller, J. (1967). A formula for average foliage density. *Australian Journal of Botany, 15*, 141-144

Myneni, R.B., Hall, F.G., Sellers, P.J., & Marshak, A.L. (1995). The interpretation of spectral vegetation indexes. *IEEE transactions on Geoscience and Remote Sensing, 33*, 481-486

Nguy-Robertson, A., Gitelson, A., Peng, Y., Viña, A., Arkebauer, T., & Rundquist, D. (2012). Green leaf area index estimation in maize and soybean: Combining vegetation indices to achieve maximal sensitivity. *Agronomy Journal, 104*, 1336-1347

Nilson, T. (1999). Inversion of gap frequency data in forest stands. *Agricultural and Forest meteorology, 98*, 437-448

Norman, J.M., & Campbell, G.S. (1989). Canopy structure. *Plant physiological ecology* (pp. 301-325): Springer

North, P.R. (1996). Three-dimensional forest light interaction model using a Monte Carlo method. *IEEE transactions on Geoscience and Remote Sensing, 34*, 946-956

Pharr, M., Jakob, W., & Humphreys, G. (2016). *Physically based rendering: From theory to implementation*. Morgan Kaufmann

Price, J.C., & Bausch, W.C. (1995). Leaf area index estimation from visible and near-infrared reflectance data. *Remote Sensing of Environment, 52*, 55-65

Richardson, A., Wiegand, C., Wanjura, D., Dusek, D., & Steiner, J. (1992). Multisite analyses of spectral-biophysical data for sorghum. *Remote Sensing of Environment, 41*, 71-82

Rondeaux, G., Steven, M., & Baret, F. (1996). Optimization of soil-adjusted vegetation indices. *Remote Sensing of Environment, 55*, 95-107

Rouse, J., Haas, R.H., Schell, J.A., & Deering, D.W. (1974). Monitoring vegetation systems in the Great Plains with ERTS. *NASA special publication, 351*, 309

Segarra, J., Buchaillot, M.L., Araus, J.L., & Kefauver, S.C. (2020). Remote sensing for precision agriculture: Sentinel-2 improved features and applications. *Agronomy, 10*, 641

Soma, M., Pimont, F., Durrieu, S., & Dupuy, J.-L. (2018). Enhanced Measurements of Leaf Area Density with T-LiDAR: Evaluating and Calibrating the Effects of Vegetation Heterogeneity and Scanner Properties. *Remote Sensing, 10*, 1580

Strahler, A.H. (1997). Vegetation canopy reflectance modeling—Recent developments and remote sensing perspectives. *Remote Sensing Reviews, 15*, 179-194

Verhoef, W. (1984). Light scattering by leaf layers with application to canopy reflectance modeling: the SAIL model. *Remote Sensing of Environment, 16*, 125-141

Verrelst, J., Malenovský, Z., Van der Tol, C., Camps-Valls, G., Gastellu-Etchegorry, J.-P., Lewis, P., North, P., & Moreno, J. (2018). Quantifying vegetation biophysical variables from imaging spectroscopy data: A review on retrieval methods. *Surveys in Geophysics*, 1-41

Verrelst, J., Muñoz, J., Alonso, L., Delegido, J., Rivera, J.P., Camps-Valls, G., & Moreno, J. (2012). Machine learning regression algorithms for biophysical parameter retrieval: Opportunities for Sentinel-2 and-3. *Remote Sensing of Environment, 118*, 127-139

Wang, K., & Dickinson, R.E. (2012). A review of global terrestrial evapotranspiration: Observation, modeling, climatology, and climatic variability. *Reviews of Geophysics, 50*

Weiss, M., Baret, F., Leroy, M., Hautecœur, O., Bacour, C., Prevol, L., & Bruguier, N. (2002). Validation of neural net techniques to estimate canopy biophysical variables from remote sensing data. *Agronomie-Sciences des Productions Vegetales et de l'Environnement, 22*, 547-554

Weiss, M., Baret, F., Smith, G., Jonckheere, I., & Coppin, P. (2004). Review of methods for in situ leaf area index (LAI) determination: Part II. Estimation of LAI, errors and sampling. *Agricultural and Forest meteorology, 121*, 37-53

Widlowski, J.-L., Robustelli, M., Disney, M., Gastellu-Etchegorry, J.-P., Lavergne, T., Lewis, P., North, P., Pinty, B., Thompson, R., & Verstraete, M. (2008). The RAMI On-line Model Checker (ROMC): A web-based benchmarking facility for canopy reflectance models. *Remote Sensing of Environment, 112*, 1144-1150

Yan, G., Hu, R., Luo, J., Weiss, M., Jiang, H., Mu, X., Xie, D., & Zhang, W. (2019). Review of indirect optical measurements of leaf area index: Recent advances, challenges, and perspectives. *Agricultural and Forest Meteorology, 265*, 390-411

Zhao, F., Gu, X., Verhoef, W., Wang, Q., Yu, T., Liu, Q., Huang, H., Qin, W., Chen, L., & Zhao, H. (2010). A spectral directional reflectance model of row crops. *Remote Sensing of Environment, 114*, 265-285